All-optical pattern recognition and image processing on a metamaterial beam splitter

Maria Papaioannou,*,† Eric Plum,*,† and Nikolay I. Zheludev*,†

†*Optoelectronics Research Centre and Centre for Photonic Metamaterials, University of Southampton, Highfield, Southampton, SO17 1BJ, UK*

‡*Centre for Disruptive Photonic Technologies, School of Physical and Mathematical Sciences and The Photonics Institute, Nanyang Technological University, Singapore 637371*

E-mail: mcp1g13@soton.ac.uk; erp@orc.soton.ac.uk; niz@orc.soton.ac.uk

Abstract

Recognition, comparison and analysis of large patterns or images are computationally intensive tasks that can be more efficiently addressed by inherently parallel optical techniques than sequential electronic data processing. However, existing all-optical image processing and pattern recognition methods based on optical nonlinearities are limited by an unavoidable trade-off between speed and intensity requirements. Here we propose and experimentally demonstrate a technique for recognition and analysis of binary images that is based on the linear interaction of light with light on a lossy metamaterial beam splitter of substantially sub-wavelength thickness. Similarities and differences between arbitrarily complex binary images are mapped directly with a camera for real-time qualitative analysis. Regarding quantitative analysis, agreement, disagreement and any other set operation between the patterns can be determined from power measurements acquired with a photodetector. In contrast to nonlinear techniques, that require high intensities to activate the nonlinear response, the image analysis method

described here can be performed at low intensities and high speed limited only by the detector noise and response time.

Keywords: pattern recognition, image analysis, coherent perfect absorption, metamaterial, metasurface, beam splitter

Recognition and processing of optical patterns and images by electronic computers is computationally demanding and requires conversion of large quantities of optical information into electronic data. Therefore, the inherent parallelism of photonic systems has long been considered to be the route towards, faster, less complex and more energy efficient, real-time pattern recognition and image processing systems. Optical Fourier techniques and spatial light modulators, have been widely employed in image processing techniques intended for medical imaging.[1,2] However, the ultimate potential of photonic systems is revealed when all-optical logic computations come into play.[3–6] All-optical pattern recognition schemes have been realized with different types of optical correlators based on photorefractive polymers,[7] semiconductor optical amplifiers,[8] delay lines and phase shifter designs.[9] Photorefraction,[10] phase-conjugation,[11] second harmonic generation,[12] vapour atomic transitions with 4-wave mixing,[13] spatial dispersers[14] and reservoir computing[15] systems have served as the basis of reliable all-optical image processors. Nevertheless, the impact of these approaches is limited by complexity as well as fundamental speed restrictions and energy requirements due to the nonlinearities involved.

Here we report binary pattern recognition and image analysis based on the linear interaction of light with light on a beam splitter consisting of a planar metamaterial (also known as metasurface). It exploits that the light-matter interaction of a film of substantially sub-wavelength thickness can be controlled by counterpropagating coherent light waves, e.g. to control absorption,[16] polarization[17] or propagation direction[18] of light. Such coherent control of light with light was recently reported in two spatial dimensions as a platform for parallel all-optical logical operations based on the theory of an idealized metasurface absorber.[3]

The theory and experiments reported here advance this concept to allow quantitative pattern recognition and image analysis on beam splitters of arbitrary loss. In our experiments, similarities and differences between binary dot patterns are recognized and satellite images analyzed by projecting reference and test images onto opposite sides of the metamaterial beam splitter using coherent light, see Fig. 1(b,c). We demonstrate that quantitative measurements of image agreement and disagreement, and indeed of any set operation between the images, can be performed by imaging the beam splitter plane onto a photodetector. This way, the relationship between any pair of binary images (containing a large amount of optical data) may be reduced all-optically to a total of 3 characteristic power values of electronic data. Furthermore, imaging onto a CCD camera reveals maps of similarities and differences. In contrast to methods based on slow and energy demanding nonlinearities and electronics, our approach is based on linear optics and therefore it is, in principle, ultrafast with up to 100 THz bandwidth[19,20] and compatible with arbitrarily low intensities down to single photons.[21]

In general, a beam splitter can be either lossless or lossy and planar metamaterials — interfaces such as plasmonic metal films of deeply sub-wavelength thickness that are structured on the sub-wavelength scale — allow the realization of beam splitters with precisely engineered transmission, reflection and absorption levels.[22] Considering illumination by a single beam of light, we define the limiting case of an ideal lossless beam splitter as an interface having 50% transmission as well as reflection, and the limiting case of an ideal lossy beam splitter as an interface having 25% transmission as well as reflection and 50% absorption, which is the maximum achievable absorption level in truly planar structures.[23] Contrary to the common belief that light beams cannot interact in linear optics, the interaction of a beam of light with a planar metamaterial beam splitter can be controlled by a second counterpropagating coherent beam of light. This becomes clear when considering two co-polarized coherent counterpropagating waves forming a standing wave with electric field nodes and anti-nodes. A planar metamaterial interacts with the electric field of a

normally incident plane wave, but its interaction with the magnetic field is prohibited as in-plane magnetic dipole modes are not supported by truly planar structures. Consequently, metasurface positioning at an electric field anti-node will enable interaction with the wave, while metasurface translation to a node will prevent light-matter interaction rendering the metasurface perfectly transparent. The position of an ideal lossless beam splitter relative to the standing wave will control how the power of the incident wave is divided between the two output beams. In contrast, for an ideal lossy beam splitter both output beams will always have the same power and the metamaterial's position relative to the standing wave will control absorption, from 0% at a node to 100% at an anti-node.

Now let us consider two binary patterns, A and B, projected by coherent light onto opposite sides of a beam splitter, where the intensities of the illuminating light beams, I_{A} and I_{B}, are chosen such that the transmitted beam A and the reflected beam B have the same intensity for single beam illumination, $I_{\mathrm{sgl}} = TI_{\mathrm{A}} = RI_{\mathrm{B}}$ for a beam splitter with intensity transmission and reflection coefficients, T and R. Across areas of pattern overlap, constructive or destructive interference of the transmitted beam A and reflected beam B will lead to addition or cancellation of the corresponding fields depending on the phase difference between the illuminating light beams, where doubled field amplitudes correspond to an intensity of $4I_{\mathrm{sgl}}$ while field cancellation implies vanishing intensity. It follows that the similarity of two patterns can be quantified by measuring the phase-dependent overall power of the output beam with a photodetector. For binary reference and test images, A and B, with illuminated areas S_{A} and S_{B}, respectively, similarities and differences can be characterized by the area $S_{\mathrm{A}\cap\mathrm{B}}$ that is illuminated by both images (agreement) and the area of $S_{\mathrm{A}\oplus\mathrm{B}}$ that is illuminated by only one image (disagreement). The area of disagreement will lead to detection of phase-independent power $I_{\mathrm{sgl}}S_{\mathrm{A}\oplus\mathrm{B}}$. In contrast, coherent interaction of light with light in areas illuminated from opposite sides yields detection of a phase-dependent power $4I_{\mathrm{sgl}}S_{\mathrm{A}\cap\mathrm{B}}\cos^2\frac{\varphi}{2}$, where φ is the phase difference between the transmitted beam A and

Table 1: **Set operations between images A and B** based on photodetector measurements of maximum and minimum power, $P_{\max}$ and $P_{\min}$, normalized by the reference power $4P_{\mathrm{A,sgl}}$ (normalized power $\tilde{P}_{\max}$ and $\tilde{P}_{\min}$, their average $\tilde{P}_{\mathrm{avg}}$ and difference $\Delta\tilde{P}$).

Area $[S_{\mathrm{A}}]$	Power measurement
S_{A}	1
S_{B}	$4\tilde{P}_{\mathrm{avg}} - 1$
$S_{\mathrm{A}} + S_{\mathrm{B}}$	$4\tilde{P}_{\mathrm{avg}}$
$S_{\mathrm{A}\cap\mathrm{B}}$	$\Delta\tilde{P}$
$S_{\mathrm{A}\cup\mathrm{B}}$	$4\tilde{P}_{\mathrm{avg}} - \Delta\tilde{P}$
$S_{\mathrm{A}\oplus\mathrm{B}}$	$4\tilde{P}_{\min}$
$S_{\mathrm{A}\setminus\mathrm{B}}$	$1 - \Delta\tilde{P}$
$S_{\mathrm{B}\setminus\mathrm{A}}$	$4\tilde{P}_{\mathrm{avg}} - 1 - \Delta\tilde{P}$

the reflected beam B. Therefore, the detected power is

$$P(\theta) = I_{\mathrm{sgl}}\left[S_{\mathrm{A}\oplus\mathrm{B}} + 4S_{\mathrm{A}\cap\mathrm{B}}\cos^2\tfrac{\varphi}{2}\right] \tag{1}$$

It is convenient to normalize the detected output power by $4P_{\mathrm{A,sgl}}$, where $P_{\mathrm{A,sgl}} = I_{\mathrm{sgl}}S_{\mathrm{A}}$ is the total detected output power when the metamaterial is illuminated by the reference image only. The normalized output power $\tilde{P}(\theta) = \frac{P(\theta)}{4P_{\mathrm{A,sgl}}}$ is

$$\tilde{P}(\theta) = \tfrac{S_{\mathrm{A}\oplus\mathrm{B}}}{4S_{\mathrm{A}}} + \tfrac{S_{\mathrm{A}\cap\mathrm{B}}}{S_{\mathrm{A}}}\cos^2\tfrac{\varphi}{2} \tag{2}$$

Normalized in this way, the size of various characteristic areas of the images relative to the area S_{A} of the reference image can be easily determined with a photodetector by measuring only the maximum $\tilde{P}_{\max}$ and minimum $\tilde{P}_{\min}$ of the phase-dependent total power of one output beam. This is illustrated by Table 1 where $\tilde{P}_{\mathrm{avg}} = (\tilde{P}_{\max} + \tilde{P}_{\min})/2$ and $\Delta\tilde{P} = \tilde{P}_{\max} - \tilde{P}_{\min}$. In particular, the sum of the illuminated areas A and B corresponds to the average power, the differences between the binary images are given by the minimum power and the overlap between the images corresponds to the phase-dependent power fluctuations.

While the above holds for any beam splitter, it is interesting to consider the limiting cases of the ideal lossless ($T = R = 50\%$) and lossy ($T = R = 25\%$) beam splitters. For coherent

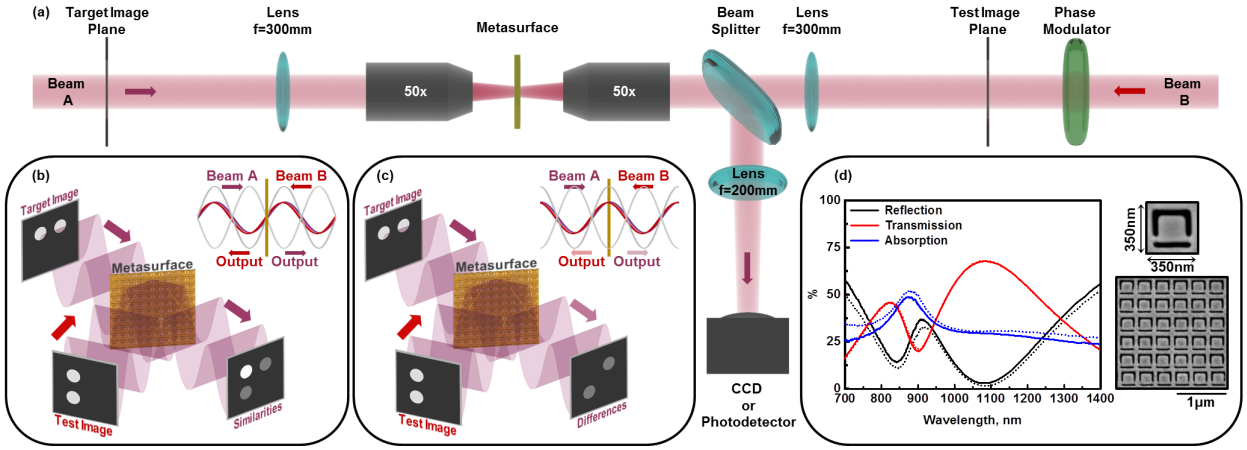

Figure 1: **Image processing setup.** (a) Schematic of the experimental setup. Target and test images, A and B, are projected onto opposite sides of a planar metamaterial beam splitter using coherent laser light of 790 nm wavelength. The metasurface is imaged onto a CCD camera. The relative beam phase difference is controlled by a phase modulator in beam B that translates the standing wave relative to the metamaterial for selective detection of (b) image similarities and (c) image differences. For the limiting case of a metasurface that is a perfect coherent absorber, similarity detector corresponds to vanishing absorption at a standing wave node and difference detection corresponds to coherent perfect absorption at an anti-node as illustrated by the insets. (d) Reflection, transmission and absorption spectra measured with illumination of front (solid lines) and rear (dotted lines) of the metamaterial. SEM images showing part of the array of asymmetrically split ring apertures in a 60-nm-thick free-standing gold film and a unit cell of the metasurface.

illumination with co-polarized counterpropagating light beams, $I_A = I_B$, the lossless beam splitter will split the incident intensity unevenly between the output beams, while the lossy beam splitter will split the incident intensity between absorption and two identical output beams. In the lossless case, coherent transparency at the standing wave node implies that the phase φ is related to the phase difference θ between the waves incident on the beam splitter by $\varphi = \theta \pm \pi/2$. In the lossy case, vanishing intensity implies coherent perfect absorption which occurs when the ideal lossy beam splitter is placed at an electric field anti-node of the standing wave formed by the incident waves, while the maximum output intensity corresponds to coherent transparency occurring when the beam splitter is placed at a node where interaction with the wave is eliminated. For such a coherent perfect absorber, the phase φ is related to the phase difference θ between the incident waves on the beam

splitter by $\varphi = \theta + \pi$.

Here we report proof-of-principle experiments demonstrating pattern recognition and image analysis using a metamaterial-based system exploiting the coherent interaction of light with light on a metasurface, see Fig. 1. The metamaterial beam splitter is a nanostructured free-standing gold film of 60 nm thickness. It was fabricated by thermal evaporation of gold on a 50-nm-thick silicon nitride membrane, followed by silicon nitride removal by reactive ion etching and nanostructuring of the remaining free-standing gold film by gallium focused ion beam milling. The gold film is perforated with an array of 350×350 nm^2 split ring apertures that has an overall size of 100×100 μm^2 and a broad resonant absorption peak around 875 nm near the experimental wavelength of 790 nm. Throughout all optical experiments, the metasurface was illuminated by linearly polarized light with the electric field oriented parallel to the symmetry axis of the split rings. The free-standing metasurface is designed to be symmetric with respect to the light propagation direction, resulting in very similar optical properties for opposite directions of illumination, see Fig. 1(d). Asymmetrically split ring aperture arrays have a rich and well-studied spectrum of transmission, reflection and absorption bands[22] and our structure absorbs about 34% at 790 nm wavelength when illuminated by a single optical beam. Thus, it is much closer to the limiting case of an ideal lossy beam splitter than the lossless one. As illustrated by Fig. 1, binary masks are positioned on the back focal plane of the imaging optics in beams A and B, aligned, and imaged onto both sides of the metamaterial using light from the same 790 nm fibre-Bragg-grating-stabilized CW diode laser with 2 mW output power and less than 0.01 nm line width. The masks were fabricated by structuring a chromium layer on a glass substrate using photolithography. While our approach will work at any intensity below damage thresholds, the laser light is attenuated to few μW to avoid detector saturation. The laser output is collimated, expanded to 12 mm diameter and then split to propagate along paths A and B of 182 cm length each, forming a standing wave where the metasurface is illuminated from both sides. The position of nodes and anti-nodes relative to the planar metamaterial is

controlled by a liquid crystal phase modulator in beam path B. The resulting coherent effects are detected in the output beam formed by the transmitted beam A and the reflected beam B by imaging the metamaterial onto a CCD camera. The input beam intensities were chosen such that the single beam transmission of beam A and reflection of beam B have the same intensity. Alignment of target and test masks must be better than their characteristic feature size to ensure that the target and test images overlap on the metasurface and misalignments are easily noticeable on the camera image. Flatness and alignment of the metasurface with respect to beams A and B is also critically important to ensure a constant phase difference between beams A and B across the metasurface beam splitter and misalignments are apparent as interference fringes on the camera image, which serves as a valuable alignment tool.

Fig. 2 illustrates binary pattern recognition for patterns of bright dots occupying 8 positions in a 4×4 grid. These may be thought of as, for example, spatially multiplexed optical data, lottery tickets or multiple choice answer sheets. A target pattern (data, winning ticket or answer sheet) is compared with test patterns with zero, partial and full agreement (row 1) by projection onto the metasurface as described above. Across areas of pattern mismatch there is no coherent interaction and therefore the detected intensity I_{sgl} is constant. In contrast, across areas of pattern agreement, coherent interaction between beams A and B on the planar metamaterial causes the detected intensity to oscillate between $4I_{\mathrm{sgl}}$ (row 2, $\varphi = 0$) and 0 (row 3, $\varphi = \pi$) as a function of the phase difference between beams A and B on the metasurface. As a result, areas of agreement are highlighted in row 2, while they are deleted from row 3, thus revealing areas of agreement (similarities) and disagreement (differences), respectively. Direct quantitative comparison of the images is most easily achieved by detecting the total power of the output beam with a photodetector. Here, we use the CCD as an effective photodetector by integrating the total power in each image. We measure (i) the output power when the metamaterial is illuminated by the reference image only $P_{\mathrm{A,sgl}}$, as well as (ii) the maximum P_{max} and (iii) minimum P_{min} output power for simultaneous metasurface illumination by reference and test images. The latter are normalized by $4P_{\mathrm{A,sgl}}$

which yields $\tilde{P}_{\max}$ and $\tilde{P}_{\min}$ as described above, see Fig. 2(b). Theory predicts that the phase-dependent power fluctuation $\Delta\tilde{P} = \tilde{P}_{\max} - \tilde{P}_{\min}$ should correspond to the fraction of the reference pattern that overlaps with the test pattern, and indeed we find that $\Delta\tilde{P}$ increases with pattern agreement. We measure $\Delta\tilde{P} = 0$ for 0% pattern agreement increasing to $\Delta\tilde{P} = 0.8$ for 100% pattern agreement, which is slightly less than the theoretical value of 1.0 due to experimental imperfections including about 1% residual transmission through nominally opaque mask areas, pattern misalignment, noise and background signals. $4\tilde{P}_{\min}$ should correspond to the area where the reference and test patterns do not overlap and for 0% pattern agreement our experiments correctly predict that the area of disagreement is twice as large as the illuminated area of the reference pattern. $\tilde{P}_{\min}$ decreases monotonously with increasing pattern overlap reaching 0.1 — slightly more than the theoretical value of zero — for complete pattern agreement. Thus, our power measurements are consistent with theory and provide quantitative measurements of the level of image agreement and disagreement with about 80% of the theoretically predicted contrast (double arrows in Fig. 2b). The experimental imperfections may be most easily taken into account by introducing an instrumental contrast correction factor f, e.g. $\tilde{P}_{\text{corr}} = f(\tilde{P}_{\text{exp}} - 0.5) + 0.5$. The ideal case corresponds to $f = 1.0$ and the contrast correction factor for our setup takes a value of about 1.2 here and about 1.1 with higher contrast masks in the case discussed below.

In order to illustrate the image analysis capabilities of our method, we use it to analyze the ice coverage evolution in the Arctic and Greenland region. We fabricated binary masks based on satellite images available from the National Snow and Ice Data Center (USA).[24] The images were taken one decade apart around the annual ice cover minimum which occurs in September from 1982 until 2012. In our experiments, we compare all satellite images (test images B) to the initial ice cover of 1982 (reference image A), see Fig. 3(a). Coherent interaction of the test and reference satellite images (row 1) on the metamaterial beam splitter clearly shows the regions where the ice cover remained unchanged (row 2) and the regions where the ice cover changed (row 3, mostly due to melting) for different phases of the

illuminating beams. Using the CCD camera as an effective photodetector, we integrate the image power to determine the maximum and minimum of the phase-dependent normalized total power, $\tilde{P}_{\max}$ and $\tilde{P}_{\min}$, as described above, see panel (b). The phase-dependent power fluctuation $\Delta\tilde{P}$ corresponds to the area of ice cover that remained unchanged, indicating that the ice cover of 1982 remained largely intact until 1992 and that substantial melting took place thereafter. However, the power fluctuation alone does not indicate growth of ice in areas that were not covered in 1982. A much more detailed analysis becomes possible when taking both $\tilde{P}_{\max}$ and $\tilde{P}_{\min}$ into account to calculate the areas where the ice cover remained, melted and grew based on Table 1. Relative to the initial ice cover of 1982 (S_{A}), the total ice cover of a test image S_{B} is given by $4\tilde{P}_{\mathrm{avg}} - 1$ and consists of the ice cover that remained unchanged $S_{\mathrm{A}\cap\mathrm{B}}$ given by $\Delta\tilde{P}$ and the ice cover $S_{\mathrm{B}\setminus\mathrm{A}}$ that grew since 1982 given by $4\tilde{P}_{\mathrm{avg}} - 1 - \Delta\tilde{P}$. The ice cover $S_{\mathrm{A}\setminus\mathrm{B}}$ that melted since 1982 is given by $1 - \Delta\tilde{P}$. Panel (c) shows the correct theory values for remaining, grown and melted ice cover in comparison to our optical experiments. Our experiments correctly reproduce the general ice cover evolution indicating that the total ice cover remains roughly constant until 1992 and then reduces by about 20% per decade. However, without applying an instrumental contrast correction factor, the areas of ice growth and ice melting are somewhat overestimated. If a contrast correction factor of $f = 1.1$ is applied to compensate for an experimental contrast of 90% rather than 100%, then the experiments reproduce the areas of ice cover that remained, melted and grew accurately.

In summary, we demonstrate all-optical binary pattern recognition and image analysis based on projecting pairs of images onto opposite sides of a metamaterial beam splitter using coherent light. In contrast to nonlinear methods, the linear technique reported here does not have fundamental minimum intensity requirements and the underlying optical effect is known to operate on the femtosecond timescale. The technique enables both real-time mapping of similarities and differences between images using a CCD camera and quantitative analysis of the relationship between pairs of images with a photodetector that could be simultaneously

achieved in a system where the output is split and directed to a CCD camera as well as a photodetector. Binary images containing a large amount of optical data can be compared all-optically and their relationship can be quantified by 3 power values of electronic data that allow the area of image overlap, areas contained in one or the other image and any other set operation to be determined. We illustrate binary pattern recognition for patterns of bright dots occupying 8 positions in a 4×4 grid and image analysis to determine the ice cover evolution in the Arctic and Greenland region based on satellite images.

Author Information

Corresponding authors

E-mail: mcp1g13@soton.ac.uk, erp@orc.soton.ac.uk, niz@orc.soton.ac.uk

Notes

The authors declare no competing financial interests.

Acknowledgement

The authors are grateful to João Valente and Edward T. F. Rogers for advice and assistance. This work is supported by the UK's Engineering and Physical Sciences Research Council (grant EP/M009122/1) and the MOE Singapore (grant MOE2011-T3-1-005). The data from this paper can be obtained from the University of Southampton ePrints research repository: http://dx.doi.org/10.5258/SOTON/403043

References

(1) Yelleswarapu, C. S.; Kothapalli, S.-R.; Rao, D. Optical Fourier techniques for medical image processing and phase contrast imaging. *Optics Communications* **2008**, *281*, 1876–1888.

(2) Yu, H.; Park, J.; Lee, K.; Yoon, J.; Kim, K. Recent advances in wavefront shaping techniques for biomedical applications. *Curr. Appl. Phys.* **2015**, *15*, 632–641.

(3) Papaioannou, M.; Plum, E.; Valente, J.; Rogers, E. T.; Zheludev, N. I. Two-dimensional control of light with light on metasurfaces. *Light Sci. Appl.* **2016**, *5*, e16070.

(4) Papaioannou, M.; Plum, E.; Valente, J.; Rogers, E. T. F.; Zheludev, N. I. All-optical multichannel logic based on coherent perfect absorption in a plasmonic metamaterial. *APL Photonics* **2016**, *1*, 090801.

(5) Fang, X.; MacDonald, K. F.; Zheludev, N. I. Controlling light with light using coherent metadevices: all-optical transistor, summator and invertor. *Light Sci. Appl.* **2015**, *4*, e292.

(6) Singh, K.; Kaur, G. Interferometric architectures based all-optical logic design methods and their implementations. *Optics & Laser Technology* **2015**, *69*, 122–132.

(7) Volodin, B. L.; Kippelen, B.; Meerholz, K.; Javidi, B.; Peyghambarian, N. A polymeric optical pattern-recognition system for security verification. *Nature* **1996**, *383*, 58–60.

(8) Yang, X.; Wu, C.; Hu, W. High-speed optical binary data pattern recognition for network security applications. *Frontiers of Optoelectronics* **2012**, *5*, 271–278.

(9) Boffi, P.; Piccinin, D.; Ubaldi, M. C.; Martinelli, M. All-optical pattern recognition for digital real-time information processing. *Appl. Opt.* **2003**, *42*, 4670–80.

(10) Ishikawa, D.; Okamoto, A.; Honma, S.; Ito, T.; Shimayabu, K.; Sato, K. All-optical multifunctional logic gates for image information using photorefractive two-wave mixing. *Optical Review* **2007**, *14*, 246–251.

(11) Norman, J. B. Phase conjugate Michelson Intereferometers for all-optical image processing and computing. *Am. J. Phys.* **1992**, *60*.

(12) Scotto, P.; Colet, P.; San Miguel, M. All-optical image processing with cavity type II second-harmonic generation. *Opt. Lett.* **2003**, *28*, 1695–7.

(13) Biaggio, I.; Partanen, J. P.; Ai, B.; Knize, R. J.; Hellwarth, R. W. Optical image processing by an atomic vapour. *Nature* **1994**, *371*, 318–320.

(14) Kim, S. H.; Goda, K.; Fard, A.; Jalali, B. Optical time-domain analog pattern correlator for high-speed real-time image recognition. *Opt. Lett.* **2011**, *36*, 220.

(15) Mesaritakis, C.; Bogris, A.; Kapsalis, A.; Syvridis, D. High-speed all-optical pattern recognition of dispersive Fourier images through a photonic reservoir computing subsystem. *Opt. Lett.* **2015**, *40*, 3416–3419.

(16) Zhang, J.; MacDonald, K.; Zheludev, N. I. Controlling light-with-light without nonlinearity. *Light Sci. Appl.* **2012**, *1*, e18.

(17) Mousavi, S. A.; Plum, E.; Shi, J.; Zheludev, N. I. Coherent control of optical polarization effects in metamaterials. *Sci. Rep.* **2015**, *5*, 8977.

(18) Shi, J.; Fang, X.; Rogers, E. T. F.; Plum, E.; MacDonald, K. F.; Zheludev, N. I. Coherent control of Snell/'s Law at metasurfaces. *Opt. Express* **2014**, *22*, 21051–21060.

(19) Fang, X.; Lun Tseng, M.; Ou, J.-Y.; MacDonald, K. F.; Ping Tsai, D.; Zheludev, N. I. Ultrafast all-optical switching via coherent modulation of metamaterial absorption. *Appl. Phys. Lett.* **2014**, *104*, 141102.

(20) Nalla, V.; Vezzoli, S.; Valente, J.; Handong, S.; Zheludev, N. I. 100 THz optical switching with plasmonic metamaterial. *CLEO/Europe-EQEC, Munich, Germany* **2015**,

(21) Roger, T.; Vezzoli, S.; Bolduc, E.; Valente, J.; Heitz, J. J. F.; Jeffers, J.; Soci, C.; Leach, J.; Couteau, C.; Zheludev, N. I.; Faccio, D. Coherent perfect absorption in deeply subwavelength films in the single-photon regime. *Nat. Commun.* **2015**, *6*, 7031.

(22) Plum, E.; Tanaka, K.; Chen, W. T.; Fedotov, V. A.; Tsai, D. P.; Zheludev, N. I. A combinatorial approach to metamaterials discovery. *J. Opt.* **2011**, *13*, 055102.

(23) Thongrattanasiri, S.; Koppens, F. H. L.; García de Abajo, F. J. Complete optical absorption in periodically patterned graphene. *Phys. Rev. Lett.* **2012**, *108*, 047401.

(24) National Snow and Ice Data Center (USA), http://nsidc.org/, `http://nsidc.org/`.

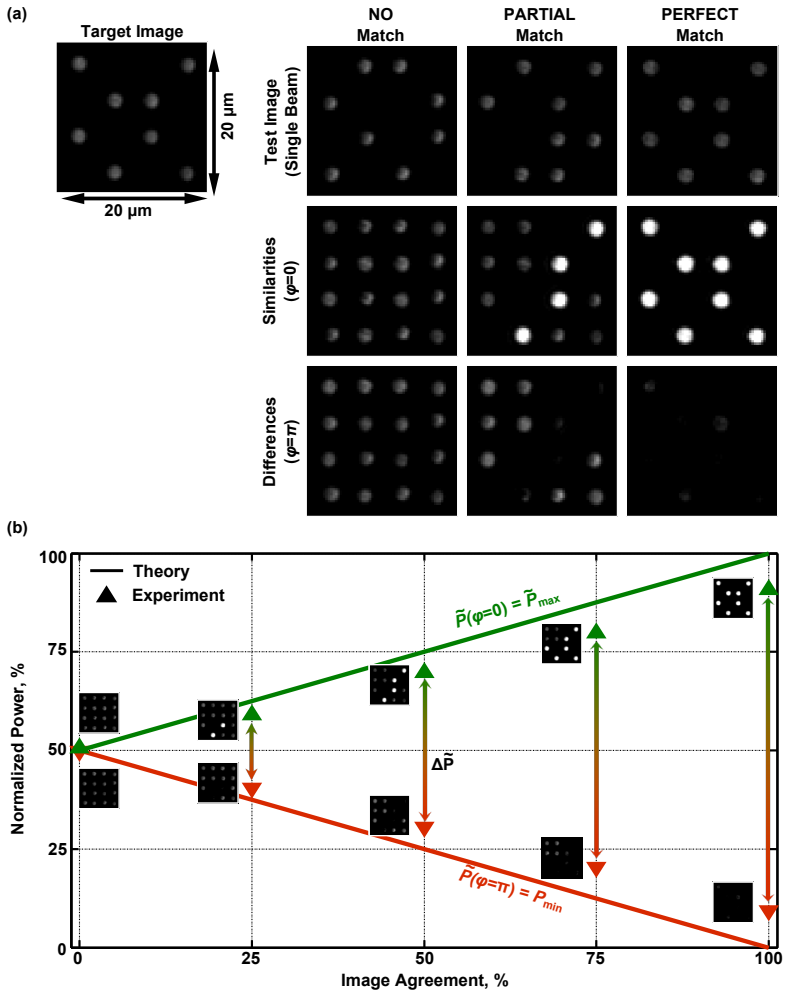

Figure 2: **All-optical pattern recognition.** (a) A target pattern is compared to a set of test patterns. The first row shows images of all patterns as captured by the CCD for single beam illumination. All test patterns are compared with the target pattern by projection onto opposite sides of the planar metamaterial using coherent light, revealing similarities (row 2) and differences (row 3) for phase differences between transmitted reference light and reflected test light of $\varphi = 0$ and π, respectively. (b) Maxima and minima of the measured (triangles) and expected (lines) total detected power normalized by $4\times$ the total target image power, $\tilde{P}$. The agreement between test and target patterns corresponds to the normalized power fluctuation, $\Delta\tilde{P}$ (double arrows).

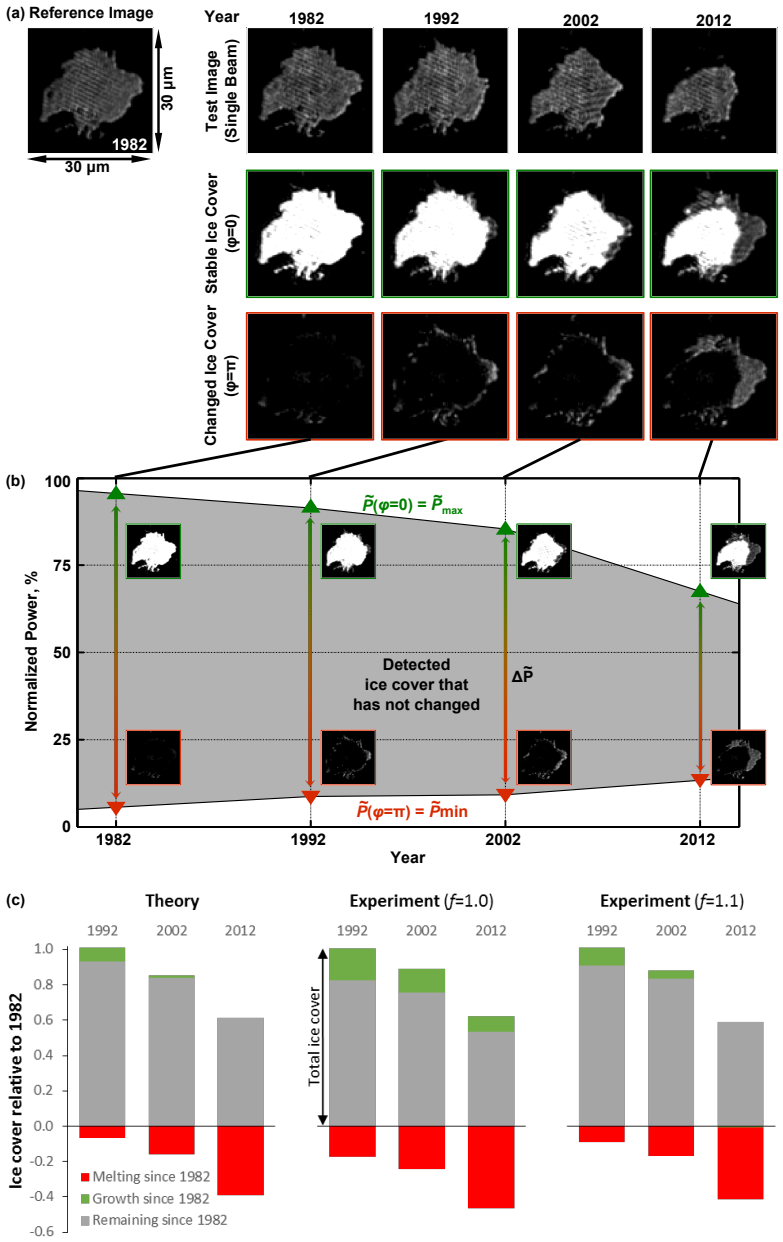

Figure 3: **Image analysis of Arctic and Greenland ice extent evolution from 1982 to 2012.** (a) Binary masks representing September ice coverage based on satellite images taken 10 years apart[24] as seen by the CCD camera for single beam illumination (row 1). Comparison to the initial 1982 ice cover by projection of the test and reference masks onto opposite sides of the metasurface using coherent light, revealing similarities (row 2) and differences (row 3) for phase differences between transmitted reference light and reflected test light of $\varphi = 0$ and π, respectively. (b) Measured normalized power $\tilde{P}_{\max}$ (green, $\varphi = 0$) and $\tilde{P}_{\min}$ (red, $\varphi = \pi$), where $\Delta\tilde{P} = \tilde{P}_{\max} - \tilde{P}_{\min}$ (arrows) corresponds to the fraction of ice cover that remained unchanged and $4\tilde{P}_{\min}$ corresponds to the fraction of ice cover change (growth or melting). The power has been determined by integrating the intensity across the corresponding image. (c) Exact theoretical and experimentally determined areas of molten $1 - \Delta\tilde{P}$, grown $4\tilde{P}_{\text{avg}} - 1 - \Delta\tilde{P}$ and remaining $\Delta\tilde{P}$ ice cover relative to the original ice cover without ($f = 1.0$) and with ($f = 1.1$) contrast correction.